Overview of Recent ICRF Studies and RF-related Wave-Field Measurements on ASDEX Upgrade

R. Ochoukov[1,a)], R. Bilato[1], V. Bobkov[1], R. Casagrande[1,2,3], H. Faugel[1], Ye. O. Kazakov[4], A. Kostic[1,2,5], M. J. Mantsinen[6,7], K. G. McClements[8], J.-M. Noterdaeme[1,2], P. Schneider[1], G. Suárez López[1,5], W. Tierens[1], M. Usoltceva[1,2,9], M. Weiland[1], W. Zhang[1], ASDEX Upgrade Team[10], EUROfusion MST1 Team[11]

[1]*Max Planck Institute for Plasma Physics, Boltzmannstr. 2, 85748 Garching, Germany*
[2]*Applied Physics Department, UGent, 9000 Gent, Belgium*
[3]*Consorzio RFX, Corso Stati Uniti 4, 35127 Padova, Italy*
[4]*Laboratory for Plasma Physics, LPP-ERM/KMS, TEC Partner, 1000 Brussels, Belgium*
[5]*Ludwig-Maximilians-University of Munich, Geschwister-Scholl-Platz 1, 80539 München, Germany*
[6]*Barcelona Supercomputing Center, Barcelona, Spain*
[7]*ICREA, Pg. Lluís Companys 23, 08010 Barcelona, Spain*
[8]*Culham Centre for Fusion Energy, Culham Science Centre, Abingdon, Oxfordshire, OX14 3DB, UK*
[9]*IJL, Université de Lorraine, 54011 Nancy, France*
[10]*see the author list in A. Kallenbach et al., Nucl. Fusion 57, 102015 (2017)*
[11]*see the author list in H. Meyer et al., Nucl. Fusion 57, 102014 (2017)*

[a)]Corresponding author: rochouko@ipp.mpg.de

Abstract. This manuscript overviews the latest developments and results from the ASDEX Upgrade ICRF team. The ICRF control system has been upgraded to allow the operation of active antennas with a controlled arbitrary phase difference between them. This upgrade, in combination with an extensive RF probe coverage inside the ASDEX Upgrade torus, makes it possible to study a global wave phenomenon that may result from the two antenna pairs' fields. The first results show that multiple active antennas form a superposition of the launched waves, with limited plasma shielding. A combination of high- and low-field side RF probes makes it possible to study the efficiency of various heating schemes such as the hydrogen minority or the 3-ion species scheme with a He-3 minority. The effect of the hydrogen minority concentration on the ICRF wave absorption and transmission through the core is best shown during conditioning discharges following a torus opening: as the hydrogen fraction is reduced from 80% to below 20%, the amplitude of the RF waves that reaches the high-field side probes is reduced by nearly two orders of magnitude indicating a strong absorption increase. The experimental results are supported by full wave FELICE code showing a similar absorption improvement as a function of the hydrogen fraction. The low-field side probes, on the other hand, do not show a sensitivity to the hydrogen fraction, which is expected as the low-field side wave amplitude is dependent on antenna coupling, not wave absorption. For the case of the 3-ion heating scheme, the high-field side probes detect a minimum in the wave amplitude as the wave absorption layer is radially scanned past the optimal position in the core. The minimum is interpreted as the optimal core absorption condition and matches the observed maximum in the core soft x-ray data. The optimal radial position of the wave absorption layer is also indirectly indicated via the appearance of strong ion cyclotron emission (ICE). The frequency of ICE is matched with the cyclotron frequency of RF-accelerated He-3 ions and the emission origin is placed ~midway between the magnetic axis and the separatrix.

In order to self-consistently assess the global ICRF wave behavior, it is necessary to account for the three dimensional (3D) nature of the toroidal tokamak plasma and the launching antenna structures. The ASDEX Upgrade ICRF team studies multiple aspects of how 3D effects influence launched ICRF wave fields and antenna performance. These include 3D

plasma density perturbations in the plasma edge and the scrape off layer, either intrinsically generated by turbulence or externally imposed by resonant magnetic perturbation coils. The experimental study is supported with RAPLICASOL: a computational tool that solves for launched ICRF wave fields in the presence of realistic 3D plasma density profiles and antenna geometry. Additionally, the work of the ASDEX Upgrade ICRF team includes fundamental plasma physics and RF wave studies on the linear test device IShTAR: the areas of interest are RF sheath rectification and arc formation.

INTRODUCTION

Ion cyclotron range of frequencies (ICRF) heating is a promising scheme to reach fusion relevant temperatures in magnetized plasmas [1]. Several shortcomings of this heating technique have recently been successfully overcome on the ASDEX Upgrade ICRF system. These include ICRF wave power coupling improvement via outer midplane gas puffing [2] and mitigation of tungsten sputtering sources from ICRF antenna limiters via a 3-strap antenna concept [3]. Despite this success, some outstanding issues still remain and are being tackled by the ICRF group on ASDEX Upgrade. These outstanding issues include the study of global ICRF wave effects generated by multiple "independent" antennas operating simultaneously [4, 5]. The interaction of launched ICRF wave fields with 3 dimensional plasma density perturbations, either applied externally with magnetic field coils [6, 7] or driven intrinsically by plasma turbulence [8], are being studied as well. ICRF heating schemes, such as the 3-ion species mechanism [9], suitable for burning tritium plasmas in next generation devices, such as ITER and DEMO, are currently under investigation on ASDEX Upgrade. Studies of a more fundamental nature, such as the interaction of the slow ICRF wave electric field with the plasma sheath [10, 11] and arc formation in the presence of ICRF fields [12], are being carried out on the IShTAR linear plasma test facility [13], and complement the overall effort of the ASDEX Upgrade ICRF team. Finally, ion cyclotron emission (ICE) intrinsically driven by the magnetized plasma in the presence of fast ions, such as fusion-born alpha particles, is being studied with the goal of developing a passive diagnostic technique to quantify the velocity distribution function of confined fast ions in the plasma core.

ICRF SYSTEM AND DIAGNOSTICS DESCRIPTION

As mentioned in the previous section, the ASDEX Upgrade tokamak is well equipped to assess ICRF-related phenomena in terms of operation, diagnostics, and computational tools. The ICRF system currently consists of 5 generators, 4 stub tuner matching networks, and 2 antenna pairs, all connected by 25-Ohm, 9-inch coaxial lines (Fig. 1). The total ICRF power delivered by the 5 generators is 5.7 MW and the operating frequencies are 30.0, 36.5, 41.8, and 55.1 MHz. One ICRF antenna pair is in a classical 2-strap balanced dipole configuration with the launched dominant parallel wave number $k_{//}$=8 m^{-1} (Fig. 2). The second antenna pair is in a 3-strap configuration, where the phase and the amplitude ratio between the central and the side straps can be arbitrarily changed. The dominant $k_{//}$ of

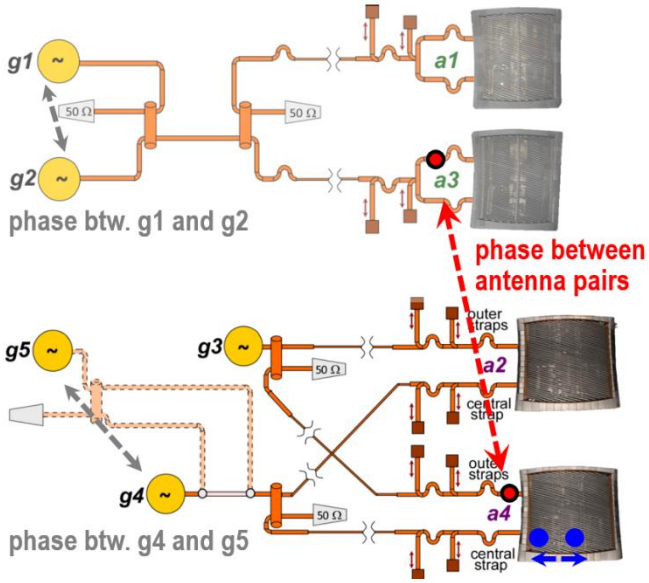

FIGURE 1. Schematic of ICRF system on ASDEX Upgrade tokamak.

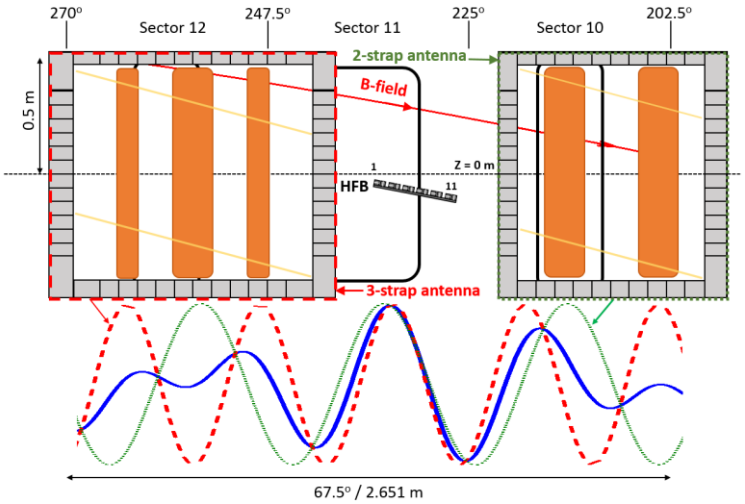

FIGURE 2. A toroidal ASDEX Upgrade outerwall view that shows the 2-strap antenna in Sector 10, the 3-strap antenna in Sector 12 and the high frequency B-dot (HFB) probe array in Sector 11. Also shown are the dominant launched parallel wave field profiles. The solid blue line is a superposition profile.

the 3-strap antenna, set in the optimal phase and amplitude ratio configuration, is 11 m^{-1} (Fig. 2). To prevent phase locking when operating the two antenna pairs simultaneously, a 1 kHz frequency difference is applied (for example, when one antenna pair operates at 30.000 MHz, the second antenna pair would run at 30.001 MHz). A recent update to the ICRF control system now makes it possible to operate the two antenna pairs at precisely equal frequencies, with a fixed controlled phase between the pairs [4]. The between-antenna pair phase is controlled at the coaxial feed points (Fig. 1), just before the RF power enters the antenna box.

To quantify the ICRF wave fields launched by the two antenna pairs, a number of B-dot probes have been installed, with extensive toroidal coverage of the ASDEX Upgrade torus on both the low- and the high-field sides (Fig. 3) [14]. The detected quantities include the amplitude, the phase, the polarization, and, in principle, the parallel wave number of the launched ICRF waves. All the quantities are sampled in the rectified DC form at 200 kHz with a slow digitizer

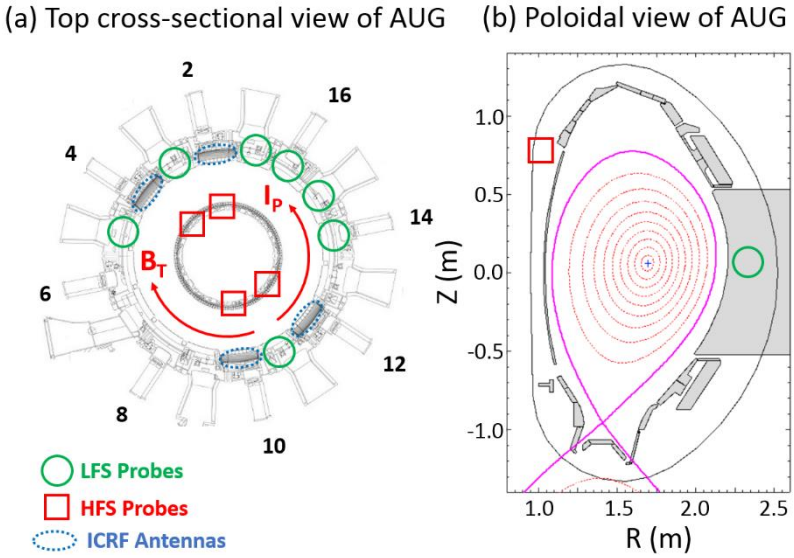

FIGURE 3. In-vessel layout of ASDEX Upgrade B-dot probes. (a) The toroidal cross sectional view and (b) the poloidal cross sectional view. The red squares indicate the high field side (HFS) probes, the green circles indicate the low field side (LFS) probes, and the dotted blue ovals indicate the ICRF antennas.

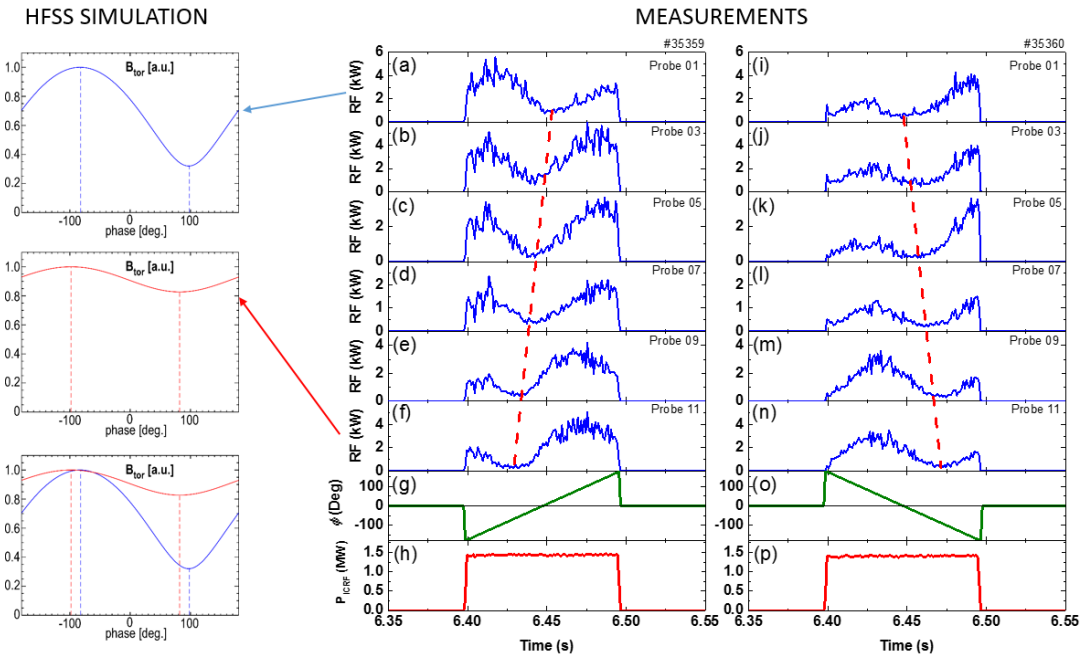

FIGURE 4. Experimental observations of wave field mixing between two active ICRF antennas on ASDEX Upgrade. (a)-(f) and (i)-(n) are RF probe signals from the HFB probe array (Fig. 2). (g) and (o) are the applied phase difference between the two active antennas and (h) and (p) are the total launched ICRF power, equally distributed between the pairs. Expected results from HFSS simulation are shown on the left column.

or with a pair of signals sampled directly at 125 MHz with a fast digitizer. A field aligned array of high frequency B-dot (HFB) probes has been installed on the low field side between the two antenna pairs (Fig. 3) specifically to measure launched $k_{//}$ spectra [15].

EXPERIMENTAL OBSERVATIONS AND NUMERICAL SIMULATION OF GLOBAL ICRF WAVE FIELDS

The global behaviour of externally launched ICRF waves in a magnetized toroidal plasma is rarely explored in tokamaks and stellarators. Limited experimental evidence is available (for example, from ASDEX Upgrade [16]) that demonstrates a non-zero effect on local RF fields and impurity sources when the phase between two active antennas is swept in a controlled manner over a 360° range. Similarly in numerical simulations, it is common practice to impose an all absorbing boundary [16] or a perfectly matched layer (PML) around an active antenna [17], effectively isolating the antenna from surrounding structures, such as other active antennas. The recent upgrade of the ICRF control system on ASDEX Upgrade [4] makes it possible to impose an arbitrary phase difference between the two ICRF antenna pairs at the feedthrough point (Fig. 1). Several discharges have been performed on ASDEX Upgrade at constant ICRF power, where the phase difference between the two antenna pairs has been continuously scanned over the full 360° range, as shown in Fig. 4. The fast wave probes on the HFB probe array, positioned toroidally between the two antenna types (Fig. 2), detect a minimum in the local ICRF wave field pattern and the minimum position varies depending on the toroidal position. Repeating the phase scan in the opposite direction reverses the dynamics of the minimum appearance on the RF probes (Fig. 4). The experimental results show good agreement with the expected global wave field behaviour based on vacuum wave field simulations with the HFSS code [4].

EXPERIMENTAL OBSERVATIONS AND NUMERICAL SIMULATION OF ICRF WAVE FIELDS DURING CONDITIONING DISCHARGES

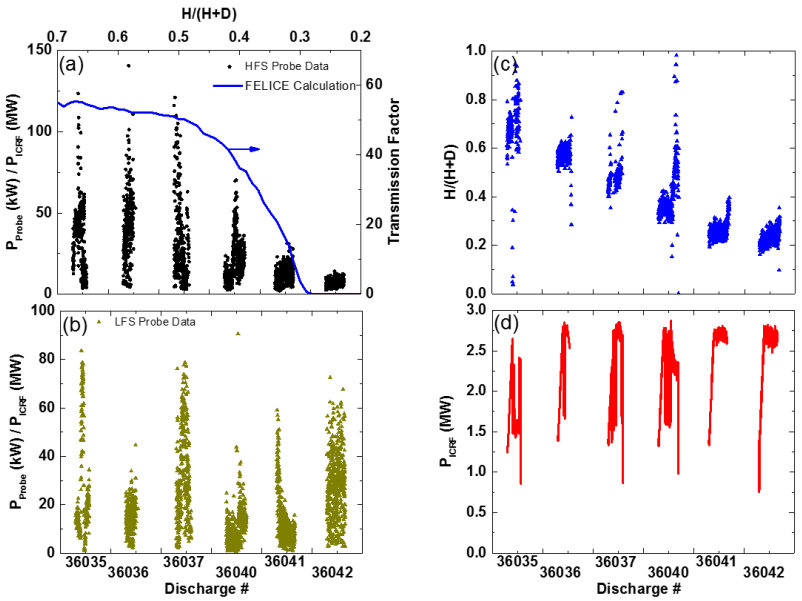

FIGURE 5. RF wave behavior during conditioning discharges. (a) The high field side probe data and FELICE simulation results; (b) the low field side probe data; (c) the hydrogen fraction evolution; and (d) the launched ICRF power.

In order to ensure optimal ICRF power absorption in the plasma core, the plasma ion composition must be properly controlled. For the case of ASDEX Upgrade, this control is achieved via torus conditioning, immediately following the vessel closure and bake. The conditioning phase normally lasts for a single day of operation and involves the application of several discharges with high auxiliary power (typically >=5 MW, enough to enter H-mode) aimed at reducing water contents in the torus wall. As the water content begins to drop, oxygen and hydrogen impurity levels in the plasma begin to fall resulting in lower oxygen radiative power losses and, for the case of ICRF power, in improved wave absorption. We quantify the ICRF wave absorption via the transmission coefficient $\eta=P_{HFS}/P_{ICRF}$, where P_{HFS} is the ICRF power that reaches the high field side wall and P_{ICRF} is the ICRF power launched by the antennas from the low field side. The launched ICRF power is directly measured by directional couplers. The relative measure of the ICRF power that reaches the inner wall is provided by the high field side B-dot probes. Although the B-dot probes are absolutely calibrated, their placement behind the heat shield tiles provides an additional uncalibrated attenuation factor. Nevertheless, the shot-to-shot evolution of the RF amplitude measured by the high field side B-dot probes during the conditioning phase is broadly consistent with how much ICRF power is absorbed by the plasma core as a function of the hydrogen contents (Fig. 5). The transmission coefficient is independently computed by the one dimensional FELICE code [18] for the experimentally relevant plasma profiles (blue line in Fig. 5 (a)). As the hydrogen concentration drops below ~30% (Fig. 5 (c)), the ICRF power absorption in the core begins to dominate (FELICE results in Fig. 5 (a)): this is indicated by the large reduction in the high field side probe data scatter and the overall low amplitude values (Fig. 5 (a)). On the other hand, the low field side probe data scatter shows no dependence on the hydrogen concentration (Fig. 5 (b)). This result is expected as the ICRF wave fields in this region are dominated by antenna coupling, which remains largely unchanged, since the same discharge recipe (with the same radial distance between the antenna and the fast wave cut off layer) is repeated over the course of the plasma conditioning phase.

EXPERIMENTAL OBSERVATIONS OF ICRF WAVE FIELDS DURING 3-ION HEATING SCENARIO DISCHARGES

The ASDEX Upgrade ICRF group is well positioned to study in detail novel fusion-relevant ICRF schemes such as the 3-ion species heating mechanism [9]. Several discharges of this variety have been successfully performed on ASDEX Upgrade at 30 MHz, involving a mix of hydrogen (~80%), deuterium (~20%), and He-3 (<1%). The scheme's efficiency is sensitive to several parameters, such as the He-3 concentration, the launched parallel wavenumber $k_{//}$, and the radial position of the wave absorption layer in the plasma core. For fixed He-3 concentration and $k_{//}$, the absorption layer position can be radially moved via a magnetic field scan (Fig. 6). The presence of an optimal absorption layer position is detected via multiple diagnostics: the core electron temperature peaks at a particular B

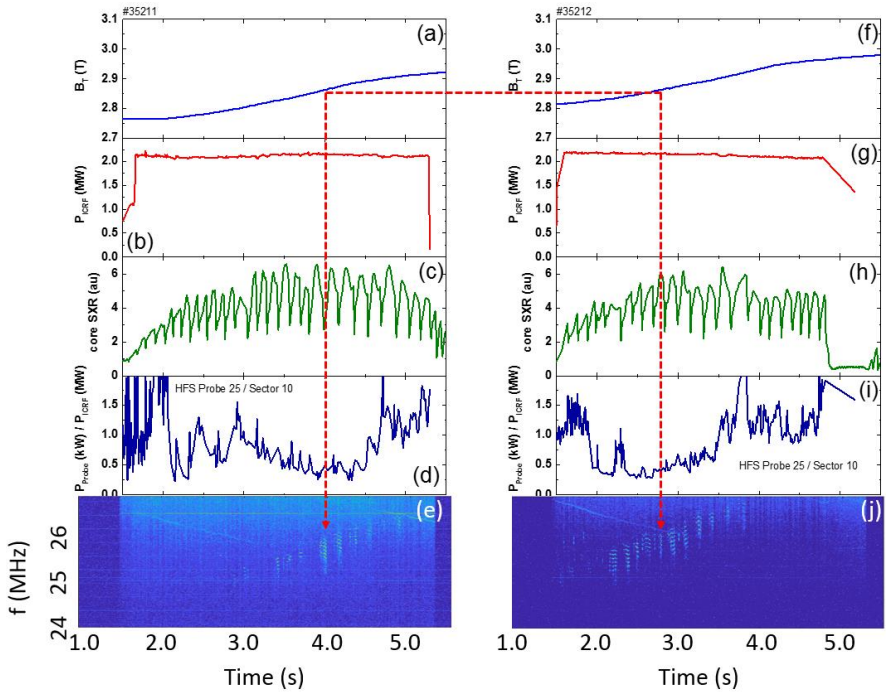

FIGURE 6. Discharge evolution during 3-ion heating. (a) and (f) On-axis magnetic field values; (b) and (g) launched ICRF power; (c) and (h) core soft X-ray signals; (d) and (i) high field side RF probe data; and (e) and (j) ion cyclotron emission spectra.

field value (Fig. 6). Additionally, the high field side probes detect a minimum in the RF wave amplitude scatter that reach the inner wall (Fig. 6). Finally, ion cyclotron emission (ICE) becomes more prominent as the magnetic field reaches its optimal value (Fig. 7).

As we already mentioned in the paragraph above, the ICRF wave field observations in ASDEX Upgrade discharges are not limited to the waves launched by the antennas: intrinsically generated ion cyclotron emission (ICE) is often observed in the presence of an inverted fast ion population. The source of the fast ion species can be either neutral beam injections, ICRF wave acceleration, or fusion reactions. For the case of the 3-ion species discharges (Fig. 6), the fast ion species is the ICRF wave accelerated He-3 ions, which can reach perpendicular energies in the range of ~1 MeV (Fig. 7 (b)) [9]. Using the ion cyclotron relation $\omega = q_{He\text{-}3}B/m_{He\text{-}3}$ (where $q_{He\text{-}3}$ is the He-3 ion charge, B is the

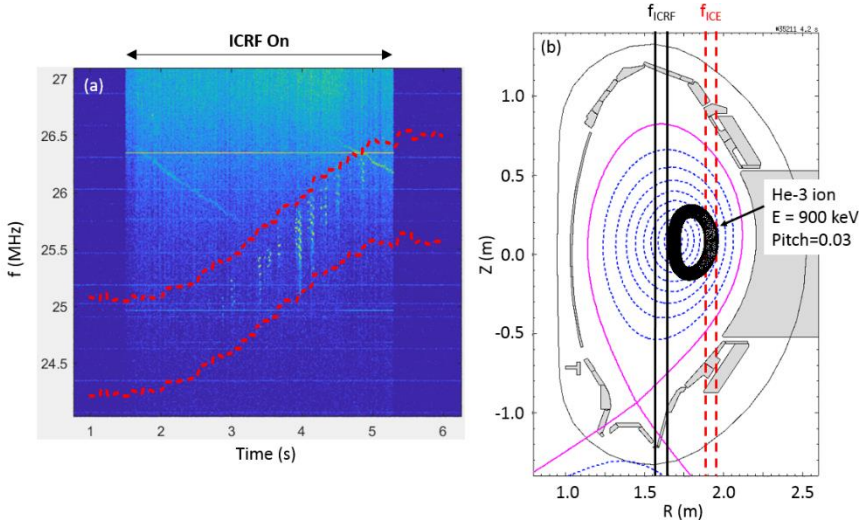

FIGURE 7. (a) Detailed view of ICE spectra from Fig. 6 (e). (b) Example of He-3 fast ion orbits consistent with ICE in (a). The red dashed lines in (a) correspond to the He-3 cyclotron frequency in the radial region indicated by the red dashed lines in (b).

local magnetic field strength, and m_{He-3} is the He-3 ion mass) and assuming a negligible drift velocity and Doppler shift contribution to the fundamental ion cyclotron resonance condition, we position the origin of ICE nearly midway between the magnetic center and the plasma separatrix at the flux averaged minor radius ρ_p ~0.5-0.6 (Fig. 7 (b)). This is in stark contrast to the classic ICE position on the low field side edge, near the separatrix [19]. In fact, recent reports of core ICE originating in the vicinity of the magnetic axis [20] demonstrate that ICE is not unique to the low field side edge region but can appear at several radial locations in the plasma spanning the entire confined region ($0 \leq \rho_p \leq 1$).

STUDIES OF ICRF WAVE FIELD INTERACTIONS WITH 3D PLASMAS

The ASDEX Upgrade tokamak is equipped with magnetic perturbation (MP) coils, which make it possible imposing a normal magnetic field to the equilibrium flux surfaces. When these perturbations are applied to ICRF-heated discharges, the ICRF power coupling is impacted and the level of impact depends on the applied 3D perturbation spectra (see [6] and references therein). The proper numerical assessment of the interaction between launched ICRF wave fields and the resulting 3D plasma density makes it necessary to couple different codes. The PARVMEC and BMW codes have been used to self-consistently compute the 3D magnetohydrodynamic equilibrium and magnetic field distribution in the scrape-off layer. A computational grid can be constructed on the basis of this field, and 3D plasma density profiles are then computed via the EMC3-EIRENE fluid transport code. As a final computational step, the plasma density profiles are input to the RAPLICASOL code, which computes the resulting ICRF antenna S-matrices, now with realistic 3D antenna structures [7]. Overall, the computed ICRF antenna loading resistance response to the applied 3D perturbations reproduces the experimentally measured trends.

3D plasma density perturbations in the antenna vicinity can also be generated intrinsically by the plasma in the form of blobs and edge localized modes (ELMs). The scattering of ICRF waves by blobs/filaments and ELMs have been studied numerically and experimentally in a tokamak environment [8]. Two numerical methods have been developed: (1) for basic wave-plasma interactions, a 2D plasma-wave interaction model in COMSOL has been developed; (2) for specific simulations of tokamaks, the 3D edge turbulence code BOUT++ which incorporates a six-field two fluid model is used to calculate the 3D perturbed scrape-off layer density in the presence of ELMs or filaments, and the RAPLICASOL code is used to calculate the 3D perturbed electric wave fields. From both basic wave-blob interaction studies and specific simulations on ASDEX Upgrade, it has been found that density blobs or density holes in the scrape-off layer can lead to global perturbations of electric fields and Poynting fluxes [8]. The parameter scan studies show that the changes of electric fields depend almost linearly on the magnitude of the density perturbations, and they depend roughly linearly on the spatial size of the ELMs or filaments when they are smaller than the radial wavelength in the propagating region ($\lambda_r \approx 0.13$ m for launched ICRF frequency f_{ICRF}=36.5 MHz).

FUNDAMENTAL STUDIES OF RF SHEATH AND ARC FORMATION ON ISHTAR

The work of the ASDEX Upgrade ICRF team also involves fundamental plasma-wave interaction studies on a linear plasma test stand IShTAR [13]. IShTAR is now equipped with a spectroscopic diagnostic to provide data on electric fields in the sheaths of its ICRF antenna. The diagnostic uses polarization Stark spectroscopy to deliver direct and localized measurements of the electric fields determined from the Stark shifts of emission spectral lines of neutral helium. The results presented at this conference [11] demonstrate the proof of principle of this technique and the diagnostic operation in non-helium plasmas. The demonstration was on two discharge configurations differing only in that the ICRF antenna was used in one and not in the other. The electric fields established across the sheath of an ICRF antenna evaluated for the two configurations differ by 0.34 kV/cm implying that even the maximum power supplied to the ICRF antenna in IShTAR, P = 1 kW, is too low for the RF sheath effects to exceed the classical thermal sheath voltage drop. These results, however, serve as a stepping-stone to further optimize ICRF discharges in IShTAR in the direction of the relevant RF sheath physics study. In addition, they contribute to the ongoing diagnostic development towards the space-resolved RF sheath electric field measurements in non-helium plasmas, for a possible implementation in tokamak antenna environments.

SUMMARY

A summary of recent work and results from the ASDEX Upgrade ICRF group has been presented. The group is well equipped with multiple operational, diagnostic, and computational ICRF tools to tackle fusion relevant challenges

[1]. Such challenges include a self-consistent assessment of the global ICRF wave field structure launched by multiple "independent" antennas (Fig. 4) [4, 5]. The efficiency of various fusion relevant scenarios, such as the hydrogen minority (Fig. 5) and the 3-ion species scheme (Fig. 6), has also been assessed experimentally and computationally. Intrinsically generated waves (ICE) are also being studied (Fig. 7) with the goal of developing a passive diagnostic method for fast ion measurements inside a deuterium-tritium burning plasma core. Interactions of launched ICRF wave fields with realistic 3D plasma density profiles are currently under investigation both experimentally [6, 8] and computationally [7]. Studies of fundamental plasma-wave interactions are being carried out on the linear plasma test stand IShTAR with the focus on RF sheath rectification [10, 11] and RF arc formation [12].

ACKNOWLEDGMENTS

This work has been carried out within the framework of the EUROfusion Consortium and has received funding from the Euratom research and training programme 2014-2018 and 2019-2020 under grant agreement No 633053. The views and opinions expressed herein do not necessarily reflect those of the European Commission.

REFERENCES

1. J.-M. Noterdaeme et al., "Fifty years of progress in ICRF, from first experiments on the Model C Stellarator to the design of an ICRF system for DEMO" review paper, these proceedings.
2. W. Zhang et al 2016 Nucl. Fusion **56** 036007.
3. V. Bobkov et al 2017 Plasma Phys. Control. Fusion **59** 014022.
4. V. Bobkov et al., "Improved operating space of ICRF system in ASDEX Upgrade" P3.26 contributed paper, these proceedings.
5. H. Faugel et al., "The Prospects of ICRF Generators" P2.17 contributed paper, these proceedings.
6. G. Suárez López et al., "Edge ICRF simulations in 3D geometry: From MHD equilibrium to coupling determination" P2.9 contributed paper, these proceedings.
7. W. Tierens et al., "Recent improvements to the ICRF antenna coupling code "RAPLICASOL"" P2.11 contributed paper, these proceedings.
8. W. Zhang et al., "Influence of ELMs on ICRF" P2.12 contributed paper, these proceedings.
9. Ye. O. Kazakov et al., Nature Physics volume **13**, pages 973–978 (2017).
10. M. Usoltceva et al., "RF sheath modelling in the presence of propagating slow wave in the conditions of IShTAR" P1.14 contributed paper, these proceedings.
11. A. Kostic et al., "Direct local electric field measurements in the sheaths of ICRF antenna in IShTAR" P1.12 contributed paper, these proceedings.
12. R. Casagrande et al., "Influence of external plasma on ICRF voltage stand-off" P1.4 contributed paper, these proceedings.
13. K. Crombe et al., "Studies of RF sheaths and diagnostics on IShTAR" AIP Conference Proceedings **1689**, 030006 (2015).
14. R. Ochoukov et al., "Major upgrades of the high frequency B-dot probe diagnostic suite on ASDEX Upgrade" EPJ Web of Conferences **157**, 03038 (2017).
15. R. Ochoukov et al., Review of Scientific Instruments **86**, 115112 (2015).
16. V. Bobkov et al 2013 Nucl. Fusion **53** 093018.
17. W. Tierens et al., Nucl. Fusion **59** (2019) 046001.
18. M. Brambilla, Plasma Physics and Controlled Fusion, Vol. **31**, No. 5. pp, 123-151, 1989.
19. G. A. Cottrell et al., 1993 Nucl. Fusion **33** 1365.
20. R. Ochoukov et al., Review of Scientific Instruments **89** 10J101 (2018).